Received: 3 October 2022 | Revised: 26 June 2023 | Accepted: 28 June 2023

DOI: 10.1002/psp4.13009

ARTICLE

Development of a multiscale mechanistic modeling framework integrating differential cellular kinetics of CAR T-cell subsets and immunophenotypes in cancer patients

Ahmed M. Salem[1,2] | **Ganesh M. Mugundu**[1] | **Aman P. Singh**[1]

[1]Clinical Pharmacology and Modeling, Precision and Translational Medicine, Oncology Cell Therapy and Therapeutic Area Unit, Takeda Pharmaceuticals, Cambridge, Massachusetts, USA

[2]Center for Translational Medicine, University of Maryland School of Pharmacy, Baltimore, Maryland, USA

Correspondence
Aman P. Singh, Clinical and Quantitative Pharmacology, Precision and Translational Medicine, Oncology Cell Therapy and Therapeutic Area Unit, Takeda Pharmaceuticals, 40 Landsdowne Street, Cambridge, MA 02139, USA.
Email: aman.singh1@takeda.com

Funding information
Takeda Development Center Americas, Inc.

Abstract

Chimeric antigen receptor (CAR) T-cell subsets and immunophenotypic composition of the pre-infusion product, as well as their longitudinal changes following infusion, are expected to affect CAR T-cell expansion, persistence, and clinical outcomes. Herein, we sequentially evolved our previously described cellular kinetic-pharmacodynamic (CK-PD) model to incorporate CAR T-cell product-associated attributes by utilizing published preclinical and clinical datasets from two affinity variants (FMC63 and CAT19 scFv) anti-CD19 CAR T-cells. In step 1, a unified cell-level PD model was used to simultaneously characterize the in vitro killing datasets of two CAR T-cells against CD19+ cell lines at varying effector:target ratios. In step 2, an augmented CK-PD model for anti-CD19 CAR T-cells was developed, by integrating CK dataset(s) from two bioanalytical measurements (quantitative polymerase chain reaction and flow cytometry) in patients with cancer. The model described the differential in vivo expansion properties of CAR T-cell subsets. The estimated expansion rate constant was ~1.12-fold higher for CAR+CD8+ cells in comparison to CAR+CD4+ T-cells. In step 3, the model was extended to characterize the disposition of four immunophenotypic populations of CAR T-cells, including stem-cell memory, central memory, effector memory, and effector cells. The model adequately characterized the longitudinal changes in immunophenotypes post anti-CD19 CAR T-cell infusion in pediatric patients with acute lymphocytic leukemia. Polyclonality in the pre-infusion product was identified as a categorical covariate influencing differentiation of immunophenotypes. In the future, this model could be leveraged a priori toward optimizing the composition of CAR T-cell infusion product, and further understand the CK-PD relationship in patients.

Study Highlights

WHAT IS THE CURRENT KNOWLEDGE ON THE TOPIC?

Heterogeneity in the product characteristics of chimeric antigen receptor (CAR) T-cells significantly influences the overall expansion, persistence, and clinical

activity. Although widely acknowledged, quantitative differences in CAR T-cell subsets and immunophenotypes kinetics post-infusion are poorly understood.

WHAT QUESTION DID THIS STUDY ADDRESS?

Using the multiscale cellular kinetic (CK)-pharmacodynamic modeling approach, this study addresses relative contribution of CAR T-cell CD4+/CD8+ cell subsets and immunophenotypes (i.e., stem cell memory [T_{SCM}], central memory, effector memory, and terminally differentiated effector cells) on overall exposure upon treatment. In addition, this study quantitatively integrates some of the CAR T-cell product attributes, such as CAR affinity, in vitro potency, and polyclonality which hold a significant translational value when understanding clinical exposure.

WHAT DOES THIS STUDY ADD TO OUR KNOWLEDGE?

Our unified mechanistic model characterizes CK of a heterogeneous CAR T-cell product integrating readouts from routine bioassays (flow cytometry and quantitative polymerase chain reaction). Upon CAR-Target engagement, the CAR-mediated expansion rate constant estimate for the CAR+CD8+ subset is higher than the CAR+CD4+ subset. Using two affinity variants of anti-CD19 CAR T-cells (FMC63 and CAT19), our model describes the clinical utility of key CAR T-cell product attributes, such as (1) CAR-affinity toward overall expansion and potency and (2) polyclonality toward enrichment of T_{SCM} phenotype in vivo.

HOW MIGHT THIS CHANGE DRUG DISCOVERY, DEVELOPMENT, AND/OR THERAPEUTICS?

With emerging clinical dataset(s) and continuous learn-confirm iterations, this modeling framework for CAR T-cells could a priori support product optimization for CD4/CD8 subsets and immunophenotypes and enhance our quantitative understanding of factors impacting exposure and response with CAR T-cell therapy.

INTRODUCTION

Chimeric antigen receptor (CAR) T-cells-based immunotherapy has emerged as a revolutionary modality in the past few years. It has demonstrated tremendous clinical outcomes in CD19 and BCMA expressing refractory hematological malignancies resulting in six CAR T-cell product approvals in the United States, and one approval(s) in China and Japan, respectively.[1] The current clinical landscape of CAR T-cell therapy is exponentially increasing with greater than or equal to 1810 distinct CAR clones under clinical development (Beacon).[2] Moreover, the field is rapidly pivoting toward treatment of solid tumors with novel engineering technologies.[3] Upon infusion, CAR T-cells exhibit a multiphasic cellular kinetic (CK) profile with four distinct phases namely: rapid distribution, expansion, contraction, and persistence.[4] Several factors have been shown to influence expansion and persistence of a CAR T-cell product post-treatment in patients. These factors could broadly be classified into (1) drug-specific factors (e.g., CAR affinity, CAR density, co-stimulatory domains, armoring, etc.),[5,6] (2) disease-specific factors (e.g., cancer type, tumor burden, etc.),[7,8] (3) product-specific attributes (CD4:CD8 ratio, immunophenotypic composition, in vitro functionalities, etc.),[9,10] and (4) treatment-specific factors (prior autologous stem cell transplantation, dose and type of lymphodepleting agent, etc.).[11] Given the high variability in the observed CK profiles following CAR T-cell product infusion, it is paramount to develop mechanistic models, which incorporate the aforementioned attributes when describing the CK-pharmacodynamic (PD) relationships of CAR T-cell therapy.[11]

Clinical evidence indicates that upon CAR-Target engagement, CAR+CD8+ T-cells show higher rate and extent of expansion in comparison to the CAR+CD4+ subsets.[9,12] Additionally, these subsets demonstrate differential tumor killing rates and potencies, because CAR+CD4+ cells produce lower levels of granzyme B required for tumor cell depletion but longer persistence in comparison to CAR+CD8+ cells.[13] The pre-infusion CD4:CD8 ratio has also been identified as a significant covariate influencing patient responses for the approved CAR T-cell therapies.[14] Similarly, the immunophenotypic composition of a cell product is known to contribute toward overall expansion and persistence,[10] where naïve-like or stem cell

memory (T_{SCM}) phenotypes have more self-renewal properties compared to terminally differentiated (T_{EFF}) CAR T-cell phenotypes.[10,15] Recently, Biasco et al. showed that the percentage of T_{SCM} phenotypic population as well as extent of polyclonality in a pre-infusion product contributed significantly toward the overall expansion and long-term persistence of a low affinity anti-CD19 CAR T-cell (CAT19) therapy.[10] Because CAR T-cell therapy is a heterogeneous product, where the composition of a product influences the overall exposure post-infusion, it becomes imperative to assess the impact of differential CKs of subsets and phenotypes after CAR T-cell treatment as part of the mechanistic model.

Different mathematical models have been published to characterize the multiphasic CK profile of CAR T-cells ranging from empirical piece-wise function to mechanistic compartmental models.[4,11,16–18] However, none of these CK/CK-PD models comprehensively accounted for (1) distinct expansion and disposition properties of each CAR T-cell subset and phenotype in peripheral blood and other sites of action and (2) integration of multiple bioanalytical measurements associated with CK of CAR T-cells in the clinic.

In our prior modeling effort, we presented a quantitative relationship, that incorporated drug-specific and system-specific factors in addition to in vitro functionalities.[19] The model accounted for the distribution of two CAR T-cell types (T_{EFF} and CAR T-cells memory [T_{EM}] cells) between blood and tissue compartments as well as the differentiation of CAR T_{EFF} cells to memory cells. CAR-target engagement in the tissue compartment led to simultaneous expansion of CAR T-cells and depletion of tumor cells. Although the model was able to capture the multiphasic CK profile, the model did not include CK of CAR T-cell CD4/CD8 subsets and immunophenotypes. Moreover, the model did not capture data from the two commonly used bioanalytical assay methods for measuring CAR T-cell levels namely: flow cytometry (FCM) reported in cells/μL, and quantitative polymerase chain reaction (qPCR) reported in transgene copies/μg gDNA.

Herein, we extended our previously published CK-PD model to integrate multiple bioanalytical measurements and differential kinetics of CAR+CD4+ and CAR+CD8+ subsets using data obtained from two affinity variants anti-CD19 CAR T-cell therapies. In a subsequent step, the model was evolved further to account for the in vivo kinetics of different immunophenotypes using a subset data obtained from CAT19-based CAR T-cell therapy. The developed multiscale mechanistic framework described in this article can be used to refine CAR T-cell infusion product composition and provide mechanistic understanding toward the exposure-response relationship.

METHODS

Preclinical and clinical datasets for model building

Digitized in vitro cytotoxicity experimental data for affinity variants anti-CD19 CAR-T cells

Data describing in vitro cytotoxicity assay measuring chromium (Cr^{51}) release at 4 h following the killing of SupT1 CD19 cell lines were digitized from published literature.[20,21] The assay assessed in vitro functionality of two affinity variants anti-CD19 CAR T-cells with similar signaling domain, identical K_{on} values but different CAR-binding affinity with a ~40-fold different K_{off} value in the two binders (i.e., FMC63 and CAT19). The experimental data were obtained through CAR T-cells and SupT1 CD19 tumor cell lines cocultures at varying effector:target (E:T) ratios 0.4:1 to 6.4:1 to obtain mean percentage of cytolysis.

Clinical studies for anti-CD19 CAR-T cells accounting for differential CKs of CAR+CD4+ and CAR+CD8+ subsets

Summary level CK datasets from two different clinical studies of Liso-cel (Lisocabtagene Maraleucel), a CAR T-cell product with predefined 1:1 ratio of CD4:CD8 cells, were digitized from multiple sources (Table 1) and utilized to develop the mechanistic CK-PD model. The first CK dataset included mean FCM-based longitudinal measurements of CAR+CD4+ and CAR+CD8+ cells after administration of Liso-cel at either 2×10^5 or 2×10^6 cells/kg in adult patients with acute lymphocytic leukemia (ALL; $n=13$ and 15 for each dose level, respectively).[9] The mean body weight of 70 kg was used as dosing amount and distributed equally (i.e., 1:1) for CD4 and CD8 subsets. The second CK dataset included median FCM based longitudinal measurements of CAR+CD3+, CAR+CD4+, and CAR+CD8+ at a dose of 50×10^6 cells and qPCR data after dosing at 50×10^6 ($n=45$), 100×10^6 ($n=176$), and 150×10^6 ($n=41$) cells in patients with diffuse large B-cell lymphoma (DLBCL).[12]

Clinical study of CAT19 CAR-T cells accounting for longitudinal changes in immunophenotypes post-infusion

Individual level CK dataset from pediatric patients with ALL ($n=14$) who received a median dose of 1×10^6 CAT19 CAR T-cells/kg was digitized (an assumed weight of 30 kg to calculate total dose amount). The digitized dataset

TABLE 1 Characteristics of clinical studies (source of data) that were used in CK-PD model building process.

Study	Population	CAR T product	Dose and number of subjects	CD4/CD8 percentage in the infusion product	Bioanalytical measurement	Reason for inclusion in the modeling step
Turtle et al.[9]	Adult ALL	Lisocabtagene maraleucel (Liso-cel)	$DL_1 = 2 \times 10^5$ cells/kg, $n = 13$ $DL_2 = 2 \times 10^6$ cells/kg, $n = 15$ Mean weight assumed to be 70 kg (data published as mean ± SEM)	50%:50%	Flow cytometry based longitudinal measurements of CAR+CD4+ and CAR+CD8+ subsets in PB	Differential expansion of CD4/CD8 subsets Figure 2a
Liso-cel BLA review[12]	Adult DLBCL	Lisocabtagene maraleucel (Liso-cel)	$DL_1 = 50 \times 10^6$ cells, $n = 45$ $DL_2 = 100 \times 10^6$ cells, $n = 176$ $DL_3 = 150 \times 10^6$ cells, $n = 41$ (Data published as median along with first and third quartiles)	50%:50%	(1) Flow cytometry based longitudinal measurements of CAR+CD3+, CAR+CD4+ and CAR+CD8+ subsets (DL_1 only) in PB (2) qPCR-based measurements of CAR transgene copies/μg gDNA (DL_1, DL_2, DL_3) in PB (LLOQ = 5 copies/μg gDNA)[a]	Differential expansion of CD4/CD8 subsets Figure 2a
Ghorashian et al.[20]	Pediatric ALL	Low affinity CAT19 anti-CD19 CAR T cell	10^6 cells/kg, $n = 14$ Median weight assumed to be 30 kg (Individual level data were available)	54.65%: 37.65%[b]	Flow cytometry (LLOQ = 1 cells/μL)[c] and qPCR-based measurement (LLOQ = 100 copies/μg gDNA)[d] of CAR T cells from PB and BM	Characterizing CK of CAT19-based CAR T-cells using the model accounting for CD4/CD8 subsets Figure 2a
Biasco et al.[10]	Pediatric ALL	Low affinity CAT19 anti-CD19 CAR T-cell	10^6 (cells/kg)[b], $n = 4$ (Individual level data was available for two persistent and two non-persistent patients)	54.65%:37.65%[b]	Percentages of CAR+T_{SCM}, CAR+T_{CM}, CAR+T_{EM} and CAR+ T_{EFF} in the infused product and different timepoints post-infusion in PB	Differentiation of different immunophenotypes (T_{SCM}, T_{CM}, T_{EM}, T_{EFF}) Figure 3

Abbreviations: ALL, acute lymphocytic leukemia; BLA, biologics license application; BM, bone marrow; CK-PD, cellular kinetic-pharmacodynamic; DL, dose level; DLBCL, diffuse large B cell lymphoma; LLOQ, lower limit of quantification; PB, peripheral blood; qPCR, quantitative polymerase chain reaction; T_{CM}, T central memory cells; T_{EFF}, T effector cells; T_{EM}, T effector memory cells; T_{SCM}, T stem cell memory cells.

[a]Data below the limit of quantification were not reported, hence, were not considered during model development.

[b]Reported median value from the study.

[c]Total of 20 (11.5%) observations (14 [14.1%] observation in PB and 6 [7.9%] observations in the BM) were below the limit of quantification.

[d]Total of 39 (17.3%) observations (24 [18%] observation in PB and 15 [16.3%] observations in the BM) were below the limit of quantification.

included FCM and qPCR-based measurements of CAR T-cells from peripheral blood (PB) and bone-marrow (BM) aspirates.[20] Besides individual CKs from all subjects, immunophenotypic composition as percentage of CAR+ T_{SCM}, central memory cell (T_{CM}), T_{EM}, and T_{EFF} in the infused product and different timepoints post-infusion was digitized from four patients (2 responders and 2 nonresponders).[10]

Development of a multiscale mechanistic CK-PD model

In step 1, a unified cell-level PD model was developed to characterize the in vitro functionalities of FMC63 and CAT19 CAR T-cells cocultured with SupT1 CD19+ tumor cell lines. As shown in Figure 1a, the model depicts the interaction between CAR T-cells (FMC63 or CAT19 construct) and SupT1 CD19 tumor cells where both cells grow with their own growth rates. Upon target engagement, the "number of CAR-Target Complexes per tumor cells (Cmplx)" drives simultaneous killing of tumor cells and the expansion of CAR T-cells. The unknown parameters that determine CAR T-cell functionality (i.e., maximum killing rate [K_{Kill}^{Max}] and in vitro potency [KC_{50}^{CAR-T}]) were estimated, whereas other system specific parameters, such as doubling times of tumor cells or CAR T-cells, CAR, and tumor associated antigen (TAA) densities, as well as binding rate constants were fixed to previously reported values (Table 2). The estimated KC_{50}^{CAR-T} values (fixed effect) from this modeling step were fixed in the subsequent in vivo model-based characterization of these CAR T-cells based on assumption(s) that (1) the TAA densities on tumor cells reflect actual antigen densities in CD19+ tumor cells in vivo as well as (2) the binding interactions within in vitro settings match the in vivo scenarios.

In step 2, our previously published CK-PD model[19] was extended by accounting for differential CKs of CAR+CD4+ and CAR+CD8+ T-cells in PB and BM compartments (Figure 2a). The model was able to characterize distinct expansion profiles for CD4+ and CD8+ subsets which maintaining similar dispositional properties.[22,23] To mimic the B-cell malignancies, a growing population of CD19+ B-cells that emerges from the BM compartment and distributes into PB was modeled. Each CAR T-cell subset could then engage with CD19+ B-cells to form CAR-Target complexes, which leads to simultaneous expansion of CAR T-cells and depletion of CD19+ B-cells. Total number of CAR-T cells in PB were linearly linked to transgene copies/μg gDNA as previously described for Tisagenlecleucel.[24]

$$\mathrm{Log}\left(\mathrm{CD3}_{\mathrm{transgene}}\right) = 7.62 + 0.85 \bullet \mathrm{Log}\left(\mathrm{CD3}_{\mathrm{flow}}\right) \quad (1)$$

All the CK parameters (fixed effects) were either estimated (as listed in Table 2) or were fixed to previously reported values or estimates obtained from prior step (EC_{50}^{Exp}, Kel_e). A random effect term was added to the first order maximum rate for tumor killing (K_{Kill}^{Max}) to account for the heterogeneity in cancer type (DLBCL vs. ALL) which was fixed to a value of 50%. This value was determined based on the difference in percentage of patients with complete remission after Liso-cel administration in both cancer types (93% for ALL and 53% for DLBCL).[9,25] The random effect model was assumed to follow log-normal distribution with a mean of zero and a standard deviation of ω on selected CK parameters as listed in Table 2. As the merged CK datasets contained two disease indications (ALL and DLBCL), disease-specific parameters were considered. Due to limited disease burden information in DLBCL patients, it was assumed that the interaction between CAR T-cells and tumor cells would only occur within the BM compartment and initial tumor burden was set to zero in PB. Within step 2, the modeling framework was implemented on combined summary level CK dataset of Liso-cel measured from FCM and qPCR to quantitatively characterize (1) differential CKs of CD4 and CD8 subsets, and (2) CK profiles from FCM and qPCR based bioanalytical measurement(s).

Similar modeling framework (Figure 2a) was used to simultaneously capture the individual CK data obtained after single dose administration of 1×10^6 cells/kg of low-affinity CAT19 CAR T-cells in pediatric patients with ALL using FCM ($n = 13$), and qPCR ($n = 14$) assays measured in PB and BM compartments. Because the CAT19 CK dataset by qPCR and FCM was not dissociating CAR+CD4+ and CAR+CD8+ fraction, the differential fold expansion rate constant between CD4+ (K_{max}^{ExpCD4}) and CD8+ (K_{max}^{ExpCD8}) was derived from prior modeling of Liso-Cel dataset, which conserves identical FMC63 binder. Throughout step 2, the data below the limit of quantification were handled using censoring or M3 method as described by beal.[26] Table 2 lists all the parameters used during CAT19 CK characterization and between subject variability (BSV) was estimated on selected CK parameters following log normal distribution with a standard deviation of ω.

In step 3, the model was evolved to account for differential kinetics of CD4/CD8 subsets and longitudinal changes of CAT19 CAR T-cell immunophenotype data in pediatric patients with ALL. Detailed CK dataset ($n = 14$) was available from all patients within the trial, whereas longitudinal changes in percentage of immunophenotypes in pre- and post-infusion samples were available from four patients. Figure 3 describes the model structure, where overall administered CAR T-cell dose was compartmentalized into different subset- and immunophenotype-species using autologous CAT19 product characteristics (listed in Table 1). Within both

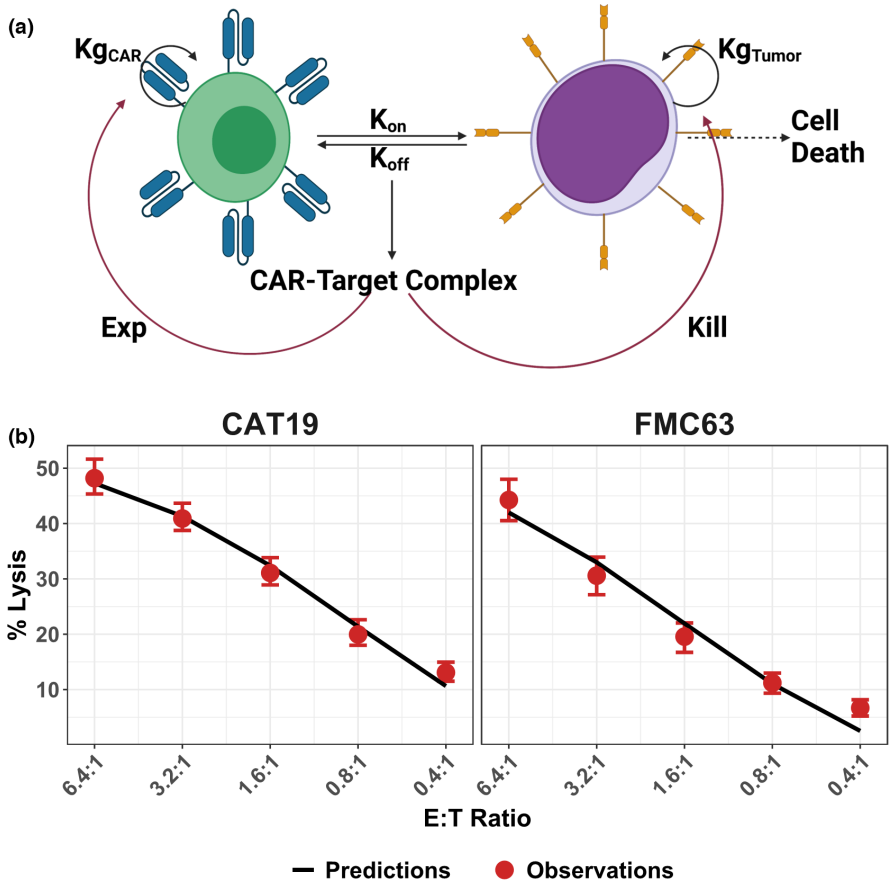

FIGURE 1 (a) Model schematics for a cell-level pharmacodynamic model to characterize the in vitro functionalities of CAR T-cells. A dynamic population of CAR-T cells and tumor cells were depicted in coculture media where both populations of cells were assumed to grow according to first order-based kinetics ($Kg_{CAR} = 0.029\,h^{-1}$ and $Kg_{Tumor} = 0.023\,h^{-1}$, respectively). Upon interaction between the effector and target cells, which is primarily governed by K_{on}/K_{off} processes, the CAR-Target complexes mediate a Michaelis–Menten-based simultaneous killing of tumor cells and expansion of CAR T-cells. (b) Observations (red dots ± standard error of the mean) and model fitted values (black lines) for the in vitro percent tumor lysis datasets obtained from CAT19 (left panel) and FMC63 (right panel) based CAR Ts: 5×10^3 tumor cells (SupT1 CD19+ cell lines) were cocultured with anti CD19 targeting CAR T-cells (carrying either CAT19 or FMC63 binders) with varying effector:target (E:T) ratios in coculture media. Tumor percent lysis was measured 4 h after coculture.

PB and BM compartments, a catenary differentiation model was implemented via which CAR T-cells differentiated from T_{SCM} phenotype to terminally differentiated T_{EFF} phenotype (Figure 3) using a series of transit rate constants (i.e., R_{m1}, R_{m2}, and R_{m3}). Median values (with standard deviations) were reported for CD4/CD8 composition in pre-infusion product, a random effect term (50%) was added to match the variability in product composition and observed CKs. Majority of the CK associated parameters for CAT19 were obtained from step 2, whereas the differentiation rate constants were estimated within this step with an assumption of 20% BSV following the US Food and Drug Administration's (FDA's) guidelines on acceptable variability for comparing exposures. Within the final model, CAR T-cell expansion was restricted to CAR+T_{SCM}+, CAR+T_{CM}+, and CAR+T_{EM}+ populations. To account for differences in immunophenotypic changes and CAR T-cell persistence between responders and nonresponders, "polyclonality" in a cell product was implemented as a categorical covariate impacting differentiation from T_{SCM} to T_{EFF} phenotypes (via R_{m1}, R_{m2}, and R_{m3}). While characterizing percentage change in immunophenotypes, an additive error model with logit-normal distribution was used to constrain the values between 0% and 100% because the observations were reported as percentages.

Because we were operating under low data environments using a mechanistic model, the performance and adequacy of the model structure was evaluated based on following criteria: (1) model fittings (i.e., observed versus predicted profiles for CK); (2) mechanistic relevance and precision on parameter estimates; and (3) ability of the model to adequately describe the multiphasic CK profile, which is the main feature of the model and characterized by rapid distribution, expansion, contraction, and persistence phases. Table 2 contains detailed information about the model parameters, and the Appendix S2 describes further details on the model

TABLE 2 List of parameters, either fixed or estimated, which were utilized to develop the preclinical (in vitro) and clinical cellular kinetic-pharmacodynamic (CK-PD) models for CAR T-cells.

Parameters associated with preclinical (in vitro) cell-level PD model (step 1; Figure 1a)				
Parameter name	**Description (units)**	**Fixed effect estimate Mean (RSE%)**	**Random effect estimate ω (RSE%)**	**Source reference**
DT^{Tumor}	The doubling time of tumor cells SupT1 CD19+ (h)	30	–	[37]
DT^{CAR-T}	The doubling time of CAR T-cells (h)	24	–	[38]
Ag^{Tumor}	Overall density of TAA (numbers/cell)	4000	–	[39]
Ag^{CAR}	Overall density of CARs on CAR T-cells (numbers/CAR T cell)	15,000	–	[19]
K_{Kill}^{Max}	The first order maximum rate of killing of tumor cells by CAR T-cells (1/h)	FMC63 = 0.24 (11.9) CAT19 = 0.22 (4.5)	–	Estimated
KC_{50}^{CAR-T}	The number of "CAR-Target Complexes per tumor cell" required to achieve 50% of the maximum killing rate (number/cell)	FMC63 = 9.16 (24.8) CAT19 = 0.28 (10.9)	–	Estimated
K_{on}	The binding affinity of CAR to TAA (1/Ms)	FMC63 = 2.07E5 CAT19 = 2.15E5	–	[20]
K_{off}	The dissociation rate of CAR to TAA (1/s)	FMC63 = 6.81E-5 CAT19 = 0.003	–	[20]
$Tumor_0$	The initial tumor cells (cell)	5000	–	[21]
V_{well}	Volume of reaction well (μL)	175	–	[21]
Parameters associated with clinical CK-PD model accounting for differential CD4/CD8 expansion (Liso-cel) (step 2; Figure 2a)				
Parameter name	**Description (units)**	**Fixed effect estimate Mean (RSE%)**	**Random effect estimate ω (RSE%)**	
K_{max}^{ExpCD8}	The first order maximum rate of CAR T-cells expansion for CAR+CD8+ subset (1/day)	2.14 (5.4)	–	Estimated
K_{max}^{ExpCD4}	The first order maximum rate of CAR T-cells expansion for CAR+CD4+ subset (1/day)	1.92 (5.8)	–	Estimated
EC_{50}^{Exp}	The number of "CAR-Target Complexes per effector cell" required to achieve 50% of the maximum rate of CAR T-cell expansion (number/cell)	10	–	19
R_m	The "net" first order conversion rate constant from effector cells to memory cells (1/day)	0.000007 (52)	–	Estimated
Kel_e	The first order elimination rate constant of effector CAR T-cells (1/day)	113	–	19
Kel_m	The first order elimination rate constant of memory CAR T-cells (1/day)	0.024 (44)	–	Estimated
K_{12}	The first order distribution rate constant from blood compartment to bone marrow compartment (1/day)	0.4 (51.8)	–	Estimated
K_{21}	The first order redistribution rate constant from bone marrow compartment to blood compartment (1/day)	0.15 (14.1)	–	Estimated
V_b	The volume of blood compartment (L)	5	–	40
V_{bm}	The volume of bone marrow compartment (L)	1.6	–	40

(Continues)

TABLE 2 (Continued)

Parameters associated with clinical CK-PD model accounting for differential CD4/CD8 expansion (Liso-cel) (step 2; Figure 2a)				
Parameter name	**Description (units)**	**Fixed effect estimate Mean (RSE%)**	**Random effect estimate ω (RSE%)**	
Ag^{CAR}	Overall density of CARs on CAR T-cells (numbers/CAR T-cell)	15,000	–	19,41
Ag^{Tumor}	Overall density of TAA on different tumor cell lines (numbers/cell)	20,000(DLBCL)/4000 (ALL)	–	39
K_{on}	The binding affinity of CAR to TAA (1/Ms)	2.07E5	–	20
K_{off}	The dissociation rate of CAR to TAA (1/s)	6.81E-5	–	20
α	The log qPCR value in copies/ μg gDNA when the log flow value in cells/μL is zero (copies/ μg gDNA)	7.62	–	24
β	The slope of linear relationship between the log qPCR value in copies/ μg gDNA and the log flow value in cells/μL (unitless)	0.85	–	24
DT^{Tumor}	The tumor doubling time (day)	29 (DLBCL)/ 5.8 (ALL)	–	42,43
K_{Kill}^{Max}	The first order maximum rate of killing of tumor cells by CAR T-cells (1/day)	1.8 (21.3)	0.5 (fixed)	Estimated
KC_{50}^{CAR-T}	The number of "CAR-Target Complexes per tumor cell" required to achieve 50% of the maximum killing rate (number/cell)	9.16	–	In vitro estimates
$K_{migration}$	The first-order trafficking constant of tumor cells from bone marrow to blood (1/day)	0.001	–	44
$IC_{Tumor\ BM}$	Initial tumor burden in bone marrow (cells/L)	5E10 (DLBCL)/1.06E11 (ALL)	–	45–47
$IC_{Tumor\ PB}$	Initial tumor burden in peripheral blood (cells/L)	0 (DLBCL)/5.5E9 (ALL)	–	48

Parameters associated with clinical CK-PD model accounting for differential CD4/CD8 expansion (CAT19) (step 2; Figure 2a])				
Parameter name	**Description (units)**	**Fixed effect estimate Mean (RSE%)**	**Random effect estimate ω (RSE%)**	
K_{max}^{ExpCD8}	The first order maximum rate of CAR T-cells expansion for CAR+CD8+ subset (1/month)	159 (17.6)	0.4 (18.3)	Estimated
K_{max}^{ExpCD4}	The first order maximum rate of CART-cells expansion for CAR+CD4+ subset (1/month)	$K_{max}^{ExpCD8}/1.12 = 142$	–	Fixed from Liso-cel estimates
PCT^{CD8}	Percentage of CD8 subset in CAR T-cell infused product (%)	38	0.5 (fixed)	20
PCT^{CD4}	Percentage of CD4 subset in CAR T-cell infused product (%)	54	0.5 (fixed)	20
EC_{50}^{Exp}	The number of "CAR-Target Complexes per effector cell" required to achieve 50% of the maximum rate of CAR T-cell expansion (number/cell)	10	–	19
R_m	The "net" first order conversion rate constant from effector cells to memory cells (1/month)	0.001 (81)	5.04 (16.6)	Estimated

TABLE 2 (Continued)

Parameters associated with clinical CK-PD model accounting for differential CD4/CD8 expansion (CAT19) (step 2; Figure 2a])				
Parameter name	**Description (units)**	**Fixed effect estimate Mean (RSE%)**	**Random effect estimate ω (RSE%)**	
Kel_e	The first order elimination rate of effector CAR T-cells (1/day)	113	–	[19]
Kel_m	The first order elimination rate constant of memory CAR T-cells (1/month)	0.39 (29.5)	1.35 (16.4)	Estimated
K_{12}	The first order distribution rate constant from blood compartment to bone marrow compartment (1/month)	3.3 (44.6)	2.08 (15.5)	Estimated
K_{21}	The first order redistribution rate constant from bone marrow compartment to blood compartment (1/day)	0.176 (fixed)	1.08 (17.8)	19
V_b	The volume of blood compartment (L)	$5 * \left(\frac{30}{70}\right)$	–	40
V_{bm}	The volume of bone marrow compartment (L)	$1.6 * \left(\frac{30}{70}\right)$	–	40
Ag^{CAR}	Overall density of CARs on CAR T-cells (numbers/CAR T-cell)	15,000	–	19,41
Ag^{Tumor}	Overall density of TAA on different tumor cell lines (numbers/cell)	4000	–	39
K_{on}	The binding affinity of CAR to TAA (1/Ms)	2.15E5	–	20
K_{off}	The dissociation rate of CAR to TAA (1/s)	0.003	–	20
α	The log qPCR value in copies/ µg gDNA when the log flow value in cells/µL is zero (copies/ µg gDNA)	7.26 (10.7)	–	Estimated
β	The slope of linear relationship between the log qPCR value in copies/ µg gDNA and the log flow value in cells/µL (unitless)	0.74 (6.9)	–	Estimated
DT^{Tumor}	The tumor doubling time (day)	10.7	–	49
K_{Kill}^{Max}	The first order maximum rate of killing of tumor cells by CAR T-cells (1/day)	1.8	–	Fixed from Liso-cel estimates
KC_{50}^{CAR-T}	The number of "CAR-Target Complexes per tumor cell" required to achieve 50% of the maximum killing rate (number/cell)	0.28	–	*Invitro* estimates
$K_{migration}$	The first-order trafficking constant of tumor cells from bone marrow to blood (1/day)	0.001	–	44
$IC_{Tumor\ BM}$	Initial tumor burden in bone marrow (cells/L)	1.06E11	–	45,47
$IC_{Tumor\ PB}$	Initial tumor burden in peripheral blood (cells/L)	1.8E9	–	50

Parameters associated with clinical CK-PD model accounting for CD4/CD8 and immunophenotypes subsets (CAT19) (step3, Figure 3)				
		Fixed effect estimate Mean (RSE%)	**Random effect estimate ω (RSE%)**	
K_{max}^{ExpCD8}	The first order maximum rate of CAR T-cells expansion for CAR+CD8+ subset (1/day)	3.44 (23.3)	0.4 (fixed)	Estimated

(Continues)

TABLE 2 (Continued)

Parameters associated with clinical CK-PD model accounting for CD4/CD8 and immunophenotypes subsets (CAT19) (step3, Figure 3)				
		Fixed effect estimate	**Random effect estimate**	
		Mean (RSE%)	**ω (RSE%)**	
K_{max}^{ExpCD4}	The first order maximum rate of CAR T-cells expansion for CAR+CD4+ subset (1/day)	$K_{max}^{ExpCD8}/1.12 = 2.9$	–	Fixed from Liso-cel estimates
PCT^{CD8}	Percentage of CD8 subset in CAR T-cell infused product (%)	38	–	20
PCT^{CD4}	Percentage of CD4 subset in CAR T-cell infused product (%)	54	–	20
EC_{50}^{Exp}	The number of "CAR-Target Complexes per effector cell" required to achieve 50% of the maximum rate of CAR T-cell expansion (number/cell)	10	–	19
R_{m1}	The first order differentiation rate constant from T_{SCM} to T_{CM} (1/day)	0.26 (21)	0.2 (fixed)	Estimated
R_{m2}	The first order differentiation rate constant from T_{CM} to T_{EM} (1/day)	0.4 (17.3)	0.2 (fixed)	Estimated
R_{m3}	The first order differentiation rate constant from T_{EM} to T_{EFF} (1/day)	0.29 (19)	0.2 (fixed)	Estimated
$\beta_{polyclonality1}$	Fractional effect of having high polyclonality on R_{m1}	0.08 (10)	–	Estimated
$\beta_{polyclonality2}$	Fractional effect of having high polyclonality on R_{m2}	0.21 (14.5)	–	Estimated
$\beta_{polyclonality3}$	Fractional effect of having high polyclonality on R_{m3}	0.19 (13.7)	–	Estimated
Kel_e	The first order elimination rate of effector CAR T-cells (1/day)	113	–	19
Kel_m	The first order elimination rate constant of memory CAR T-cells (1/day)	0.013	1.35 (fixed)	Fixed from CAT19 estimates
K_{12}	The first order distribution rate constant from blood compartment to bone marrow compartment (1/day)	0.11	2.08 (fixed)	Fixed from CAT19 estimates
K_{21}	The first order redistribution rate constant from bone marrow compartment to blood compartment (1/day)	0.176	1.08 (fixed)	Fixed from CAT19 estimates
V_b	The volume of blood compartment (L)	$5\times\left(\frac{30}{70}\right)$	–	40
V_{bm}	The volume of bone marrow compartment (L)	$1.6\times\left(\frac{30}{70}\right)$	–	40
Ag^{CAR}	Overall density of CARs on CAR T-cells (numbers/CAR T-cell)	15,000	–	19,41

TABLE 2 (Continued)

Parameters associated with clinical CK-PD model accounting for CD4/CD8 and immunophenotypes subsets (CAT19) (step3, Figure 3)				
		Fixed effect estimate	**Random effect estimate**	
		Mean (RSE%)	**ω (RSE%)**	
Ag^{Tumor}	Overall density of TAA on different tumor cell lines (numbers/cell)	4000	–	39
K_{on}	The binding affinity of CAR to TAA (1/Ms)	2.15E5	–	20
K_{off}	The dissociation rate of CAR to TAA (1/s)	0.003	–	20
DT^{Tumor}	The tumor doubling time (day)	10.7	–	49
K_{Kill}^{Max}	The first order maximum rate of killing of tumor cells by CAR T-cells (1/day)	1.8	–	Fixed from Liso-cel estimates
KC_{50}^{CAR-T}	The number of "CAR-Target Complexes per tumor cell" required to achieve 50% of the maximum killing rate (number/cell)	0.28	–	*Invitro* estimates
$K_{migration}$	The first-order trafficking constant of tumor cells from bone marrow to blood (1/day)	0.001	–	44
$IC_{Tumor\ BM}$	Initial tumor burden in bone marrow (cells/L)	1.06E11	–	45,47
$IC_{Tumor\ PB}$	Initial tumor burden in peripheral blood (cells/L)	1.8E9	–	50

Abbreviations: ALL, acute lymphocytic leukemia; CAR-T-cell, chimeric antigen receptor T-cell; CK-PD, cellular kinetic-pharmacodynamic; DLBCL, diffuse large B cell lymphoma; qPCR, quantitative polymerase chain reaction; Rm, transit rate constants; RSE, relative standard error; TAA, tumor associated antigen; T_{CM}, T central memory cells; T_{EFF}, T effector cells; T_{EM}, T effector memory cells; T_{SCM}, T stem cell memory cells.

equations, assumptions, and approaches toward parameter estimation.

RESULTS

A cell-level PD model to characterize in vitro functionalities of CAR T-cells

Figure 1b shows the model fitted profiles overlaid with observed data for percentage lysis of SupT1 CD19+ cell lines, following coculture with CAT19-based (left panel) and FMC63-based (right panel) CAR T-cells at different E:T ratios. The estimated KC_{50}^{CAR-T} for CAT19 was 0.28 number of complexes/cells compared to 9.16 complexes/cells for FMC63 indicating higher killing potency associated with low affinity CAT19 CAR T-cells (~32.7-fold compared to FMC63-based CAR T-cells).[20]

Multiscale mechanistic CK-PD model describing differential CK of CD4+ and CD8+ CAR T-cells and CD19+ B-cell dynamics

Figure 2b1 Left panel shows the model-based predictions overlaid by the observations of median CD3+, CD4+, and CD8+ longitudinal profiles for the adult patients with DLBCL who received single 50×10^6 cells of Liso-cel. Figure 2b1 middle and right panels describe the model-based predictions overlaid by mean observations of CD4+ and CD8+ subsets for adult patients with ALL who received 2×10^5 cells/kg (dose level 1) or 2×10^6 cells/kg (dose level 2). In general, the model adequately characterizes the overall CK profile (CD3+ T cells) in the DLBCL population as well the CD3+CD4+ profiles (except for CD4+ profile of dose level 2 where the model tends to overpredict the profile at the persistence phase)

(a)

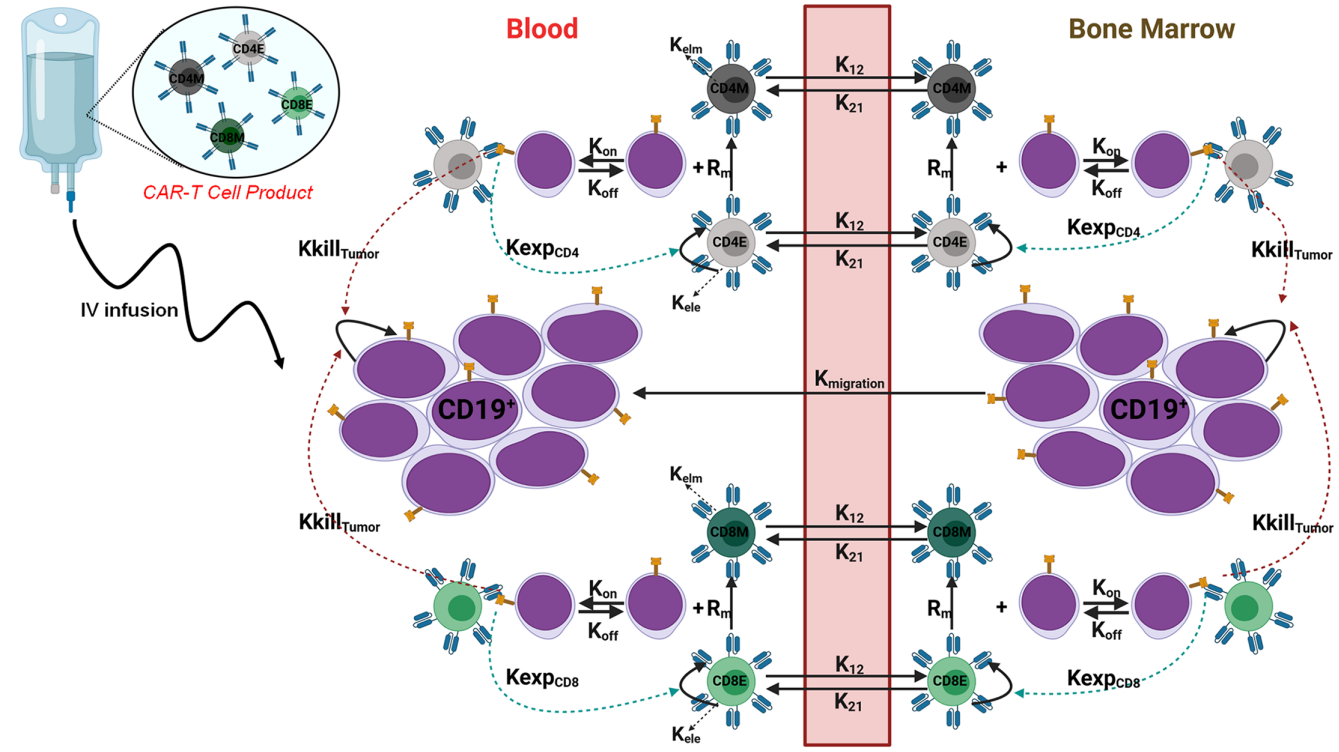
Blood
Bone Marrow
CD4M
CD4E
CD8E
CD8M
CAR-T Cell Product
IV infusion
Kelm
K12
K21
Kon
Koff
+Rm
Rm
Kexp CD4
Kexp CD8
Kkill Tumor
Kele
Kmigration
CD19+

(b1)

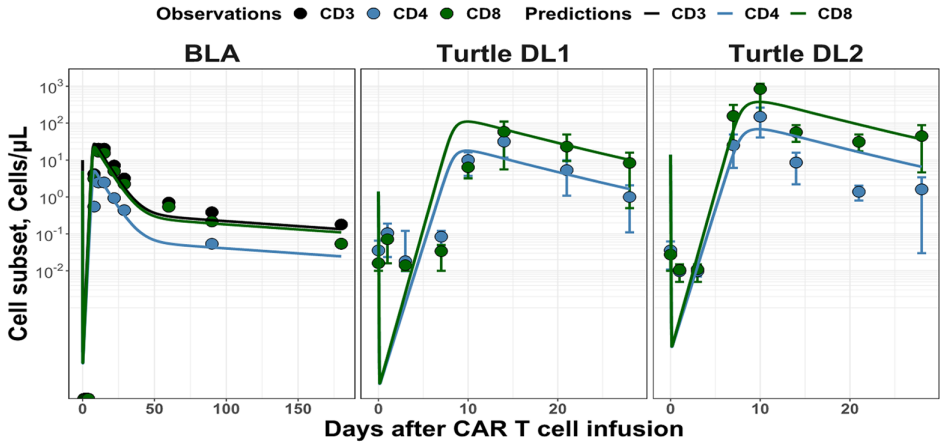
Observations CD3 CD4 CD8 Predictions CD3 CD4 CD8
BLA
Turtle DL1
Turtle DL2
Cell subset, Cells/µL
Days after CAR T cell infusion

(b2)

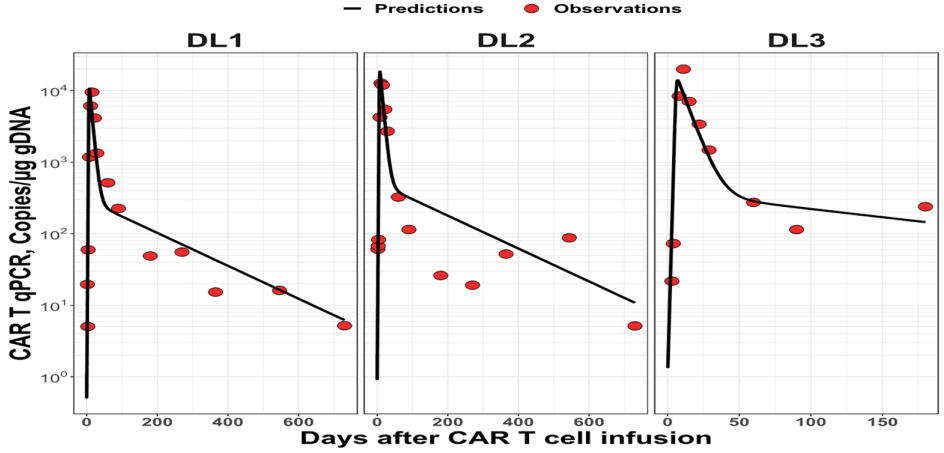
Predictions Observations
DL1
DL2
DL3
CAR T qPCR, Copies/µg gDNA
Days after CAR T cell infusion

FIGURE 2 (a) Schematics of a multiscale mechanistic CK-PD model describing differential cellular kinetics of CD4+ and CD8+ CAR T-cells and CD19+ B-cell dynamics: The developed CK-PD model has two major compartments namely: peripheral blood (PB) and bone-marrow (BM) (or the tissue compartment). Upon infusion of a heterogeneous CAR T-cell product, with a predefined ratio of CD4:CD8 subsets, both effector- and memory-phenotypes of each subset of CAR T-cells were assumed to exhibit 1st order elimination rates (via Kel_e and Kel_m) from the PB compartment and distribution rates (via K_{12} and K_{21}) to BM and back to PB, respectively. CD19+ B-cells were assumed to have first order growth kinetics both in PB and BM as well as unidirectional trafficking from BM to PB through first order constant $K_{migration}$. Within both PB and BM, effector CD4+ and CD8+ CAR T-cells differentiate into memory CAR T-cell phenotypes using a "net" first order differentiation rate constant (R_m). In both PB and BM, total CAR-T cells of CD4/CD8 subsets interact with tumor cells and form "CAR-Target complexes," which drives simultaneous expansion of effector CAR T-cells (with differential expansion rate constants for CD4/CD8 subpopulations) and killing of the CD19+ malignant B-cell population. (b) Characterization of differential clinical cellular kinetics of CD4+ and CD8+ subsets of Lisocabtagene Maraleucel (Liso-cel, 1:1 dose ratio of CD4:CD8) using a multiscale mechanistic CK-PD model. (b1) Model fittings for flow-cytometry (FCM) based bioanalytical measurements of cellular kinetics for CD4+, CD8+ and CD3+ subsets of CAR T-cells: Observed (in dots ± standard error of the mean) and model fitted profiles (lines) of CD3 + CAR+ (in black), CD4 + CD3 + CAR+ (in blue) and CD8 + CD3 + CAR+ (in green) populations of Liso-cel in peripheral blood. The left panel displays the median CK profiles of patients with DLBCL who received 50×10^6 cells ($n=45$) CAR+ cells. The other two panels show the mean cellular kinetic profiles of adult patients with ALL who received dose level one (DL1) of 2×10^5 cells/kg (middle panel) or DL2 of 2×10^6 cells/kg (right panel). (b2) Model fittings for qPCR-based bioanalytical measurements of CKs of CAR T-cells. Observed (red dots) and model-predicted profiles (black lines) of peripheral blood cellular kinetics of Liso-cel depicted in CAR transgene copies/ μg gDNA (LLOQ = 5 copies/μg gDNA). The left, middle, and right panels show the CKs in patients with DLBCL upon single infusion of Liso-cel at 50×10^6 cells ($n=45$), 100×10^6 cells ($n=176$), and 150×10^6 cells ($n=41$), respectively. The plots as inserted in each panel show the model-predicted profiles depicting the expansion phase after CAR T-cell infusion. Figure b1 left panel and Figure b2 do not include error bars because they were not reported in the original publication. ALL, acute lymphocytic leukemia; CK, cellular kinetic; DLBCL, diffuse large B-cell lymphoma; LLOQ, lower limit of quantification; PD, pharmacodynamic; CK, cellular kinetic; qPCR, quantitative polymerase chain reaction.

and CD3+CD8+ profiles for both patients with DLBCL and patients with ALL.

The CK profiles show distinctive rapid distribution, expansion, contraction, and persistence phases. Figure 2b2 shows the model fits for CK by qPCR-based measurements (transgene copies/μg gDNA) for Liso-cel doses of 50×10^6 (left panel), 100×10^6 (middle panel), or 150×10^6 (right panel) cells in patients with DLBCL. Overall, the model was able to simultaneously describe flow- and qPCR-based CK datasets for Liso-cel. The estimate for first-order maximum expansion rate for CD8 subset (K_{max}^{ExpCD8}) was $2.14\,h^{-1}$ versus $1.92\,h^{-1}$ for CD4 subset (K_{max}^{ExpCD4}), which indicates 1.12-fold higher expansion for CAR+CD8+ compared to CAR+CD4+ cells.

Similarly, the individual CK profiles for CAT19 CAR T-cells in in pediatric patients with ALL were adequately characterized by the model (Figure 4) in both PB and BM compartments. A linear relationship (as described in Equation 1) was utilized to simultaneously characterize FCM and qPCR-based datasets. The estimated intercept and slope were 7.26 copies/μg gDNA and 0.74, respectively, which is similar to previously reported values for tisagenlecleucel (7.62 copies/μg gDNA and 0.85 for intercept and slope, respectively).[24]

The maximum expansion rate constant (K_{max}^{ExpCD8}) for CAR+CD8+ fraction of CAT19 CAR T-cells was $5.3\,day^{-1}$ versus $2.14\,day^{-1}$ for Liso-cel reflecting higher overall rate of expansion for low-affinity CAT19 CAR T-cells in comparison to FMC63 based CD19 CAR T-cells. Additionally, model estimates showed slower elimination rate constant of memory cells ($0.013\,day^{-1}$ vs. $0.024\,day^{-1}$) and higher conversion rate constant from effector to memory cells ($0.000037\,day^{-1}$ vs. $0.000007\,day^{-1}$) suggested a prolonged persistence of CAT19 CAR T-cells in comparison to Liso-cel.

Multiscale mechanistic CK-PD model describing longitudinal changes in CAR T-cell immunophenotypes in patients with cancer

Our final iteration of the model (in Figure 3) was able to characterize the differential CKs of CD4/CD8 subsets and longitudinal changes of CAR T-cell immunophenotypes for CAT19 CAR T-cells in pediatric ALL population. Figure 5 describes the model-fitted profiles overlaid with observed percentage change in four immunophenotypic populations (i.e., CAR+T_{SCM}+ [panel A], CAR+T_{CM}+ [panel B], CAR+T_{EM}+ [panel C], and CAR+ T_{EFF}+ [panel D]) for four out of 14 pediatric patients with ALL administered with CAT19-based CAR T-cell therapy. Upon infusion, the T_{CM} population instantly transforms into T_{EM} population during the expansion phase of CAR T-cells. Furthermore, CAR+T_{SCM} percentage in the infusion product is low and it increases over time specifically for patients who demonstrate persistence which indicates the importance of this immunophenotypic population in driving CAR T-cell persistence. The expansion rate constant (K_{max}^{ExpCD8}) was

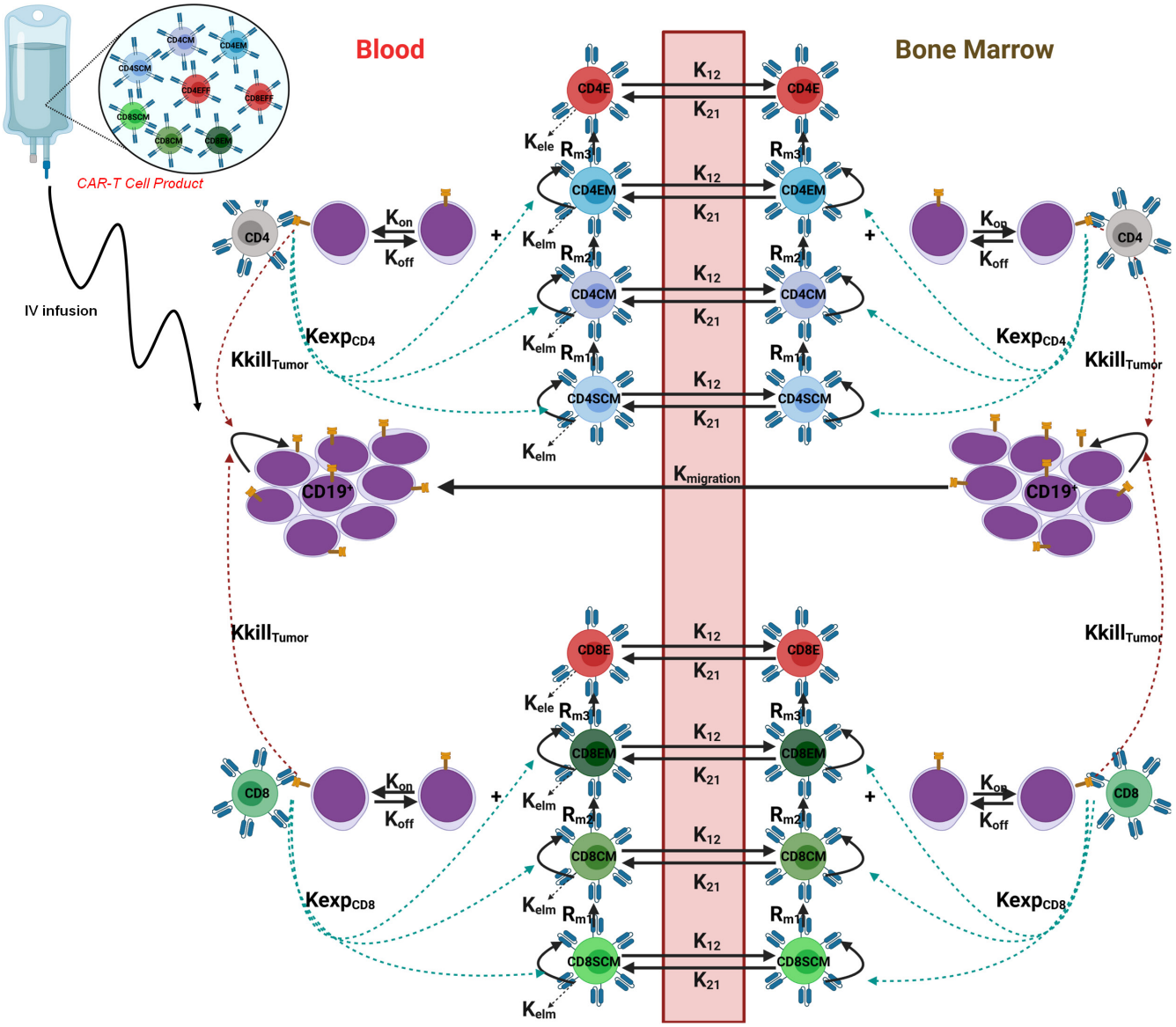

FIGURE 3 Schematics of a multiscale mechanistic CK-PD model describing differential CKs of CAR T-cells subsets and immunophenotypes in patients. The model has two compartments namely: peripheral blood (PB) and bone-marrow (BM; or the tissue compartment). The CAR T-cell product infused in the PB is assumed to be heterogeneous mixture with different proportion of CAR T-cell subsets (CD4/CD8 ratios) and immunophenotypes (i.e., stem cell memory [T_{SCM}], central memory [T_{CM}], effector memory [T_{EM}], and terminally differentiated effector [T_{EFF}] phenotypes). Each subpopulation is modeled to distribute to BM using first order distribution rates (K_{12} and K_{21}) and eliminate from PB using first order elimination rate constants (Kel_e for T_{EFF} and Kel_m for T_{SCM}, T_{CM}, and T_{EM}, respectively). CD19+ B-cells were assumed to have growth kinetics in PB and BM and trafficking from BM to PB through first order constant $K_{migration}$. Within both PB and BM, a transit compartment-based differentiation model is assumed for each CAR T-cell subset (CD4/CD8), where T_{SCM} differentiates into T_{CM}, T_{CM} differentiates into T_{EM} and T_{EM} terminally differentiates into T_{EFF} through first order differentiation rate constants ($R_{m1,}$ R_{m2}, and $R_{m3,}$ respectively). Within each compartment (PB and BM), total CAR T-cells interact with tumor cells to form "CAR-Target complexes," which drives simultaneous killing of CD19+ B-cells and expansion of CAR T-cells with T_{SCM}, T_{CM}, and T_{EM} phenotypes with differential expansion rate constants for CD4 and CD8 subpopulations. CK, cellular kinetic; PD, pharmacodynamic.

assumed to be similar across different immunophenotypes (i.e., CAR+T_{SCM}+, CAR+T_{CM}+, and CAR+T_{EM}+), whereas terminally differentiated effectors (T_{EFF}+) were modeled not to proliferate. The differentiation rate constants R_{m1}, R_{m2}, and R_{m3} were estimated to 0.26 day^{-1}, 0.4 day^{-1}, and 0.29 day^{-1}, reflecting fastest transition from CAR+T_{CM}+ to CAR+T_{EM}+, as reflected in the dataset (Figure 5).

The autologous drug product of patient IDs 4 and 6 constituted higher polyclonality and demonstrated superior CAR T-cell persistence in comparison to patient IDs 10 and 17, where persistence was limited. The model was

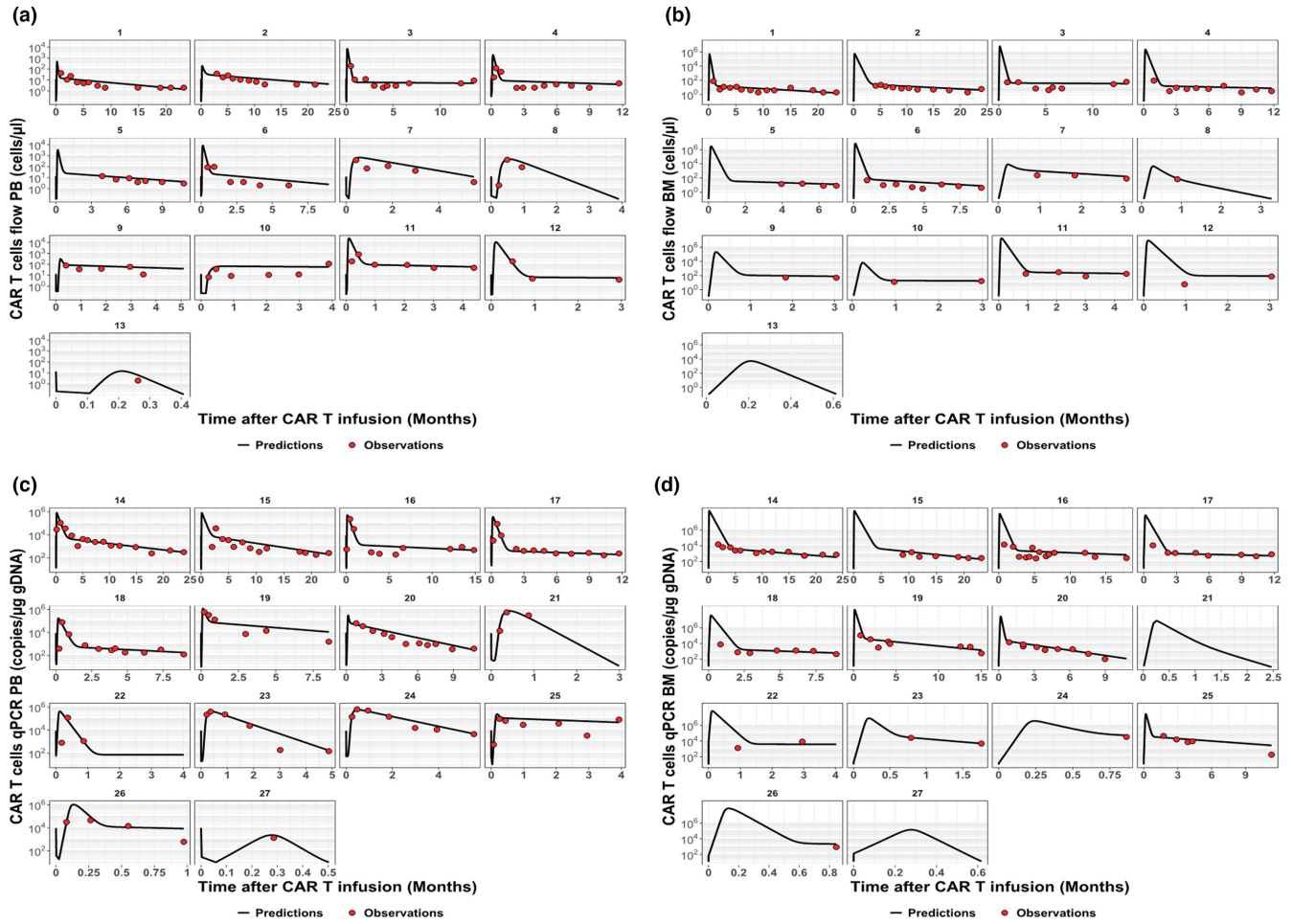

FIGURE 4 Characterization of differential clinical CKs of CD4+ and CD8+ subsets of low affinity CAT19 based anti-CD19 CAR T-cells using a multiscale mechanistic CK-PD model. Flow cytometry (FCM) based cellular kinetics of anti-CD19 CAR-Ts. (a) Observed (in dots) and model fitted profiles (lines) for individual ALL patient cellular kinetics (LLOQ = 1 CAR+ cell/µL, $n = 13$) in PB and (b) BM. The qPCR-based CKs of anti-CD19 CAR T-cells. (c) Observed (in dots) and model fitted profiles (lines) for individual patients with ALL patient CKs (LLOQ = 100 copies/µg gDNA, $n = 14$) in PB and (d) BM. The patients received a median dose of 10^6 CAR+ cells/kg. The median CD4+ percentage in the infused product was 54.65% in comparison to 37.65% for CD8+ CAR+ cells. ALL, acute lymphocytic leukemia; BM, bone marrow; CK, cellular kinetic; LLOQ, lower limit of quantification; PB, peripheral blood; PD, pharmacodynamic; qPCR, quantitative polymerase chain reaction.

able to simultaneously capture all the longitudinal in vivo percentage change for each immunophenotypic population in the four subjects by incorporating polyclonality as a categorical covariate accounting for lesser terminal differentiation for responders compared to nonresponders.

DISCUSSION

CAR T-cell therapy has recently become a pivotal therapeutic option in refractory hematological malignancies[1] with astonishing clinical outcomes and survival benefits and slowly pivoting toward solid tumors.[27] In numerous CAR T-cell clinical trials, adequate expansion and persistence of CAR T-cells has been shown to be a crucial element of improved clinical outcomes. As a heterogeneous autologous T-cell product, the CD4/CD8 subsets and immunophenotypic composition in the pre-infusion material are shown to influence the CK expansion and persistence in vivo.[10,11] Quantitatively characterizing different subsets and immunophenotypes using mechanistic models would help optimizing CAR T-cell products.[28]

Studies have shown distinct cellular expansion and tumor killing characteristics for CD4 and CD8 subsets. In the study by Macallan et al., CD8+ cells expanded at a rate of 5.1% day^{-1}, whereas CD4+ cells expanded at a rate of 2.7% day^{-1}.[29] Furthermore, pharmacometric analysis by Mueller-Schoell et al. showed that the exponent of covariate effect of CAR+ CD4/CD8 ratio at day 7 on maximum expansion rate was −0.385.[11] Hence, maximum expansion rate decreases as the ratio of CAR+CD4+ cells to CAR+CD8+ increases. There are several CAR

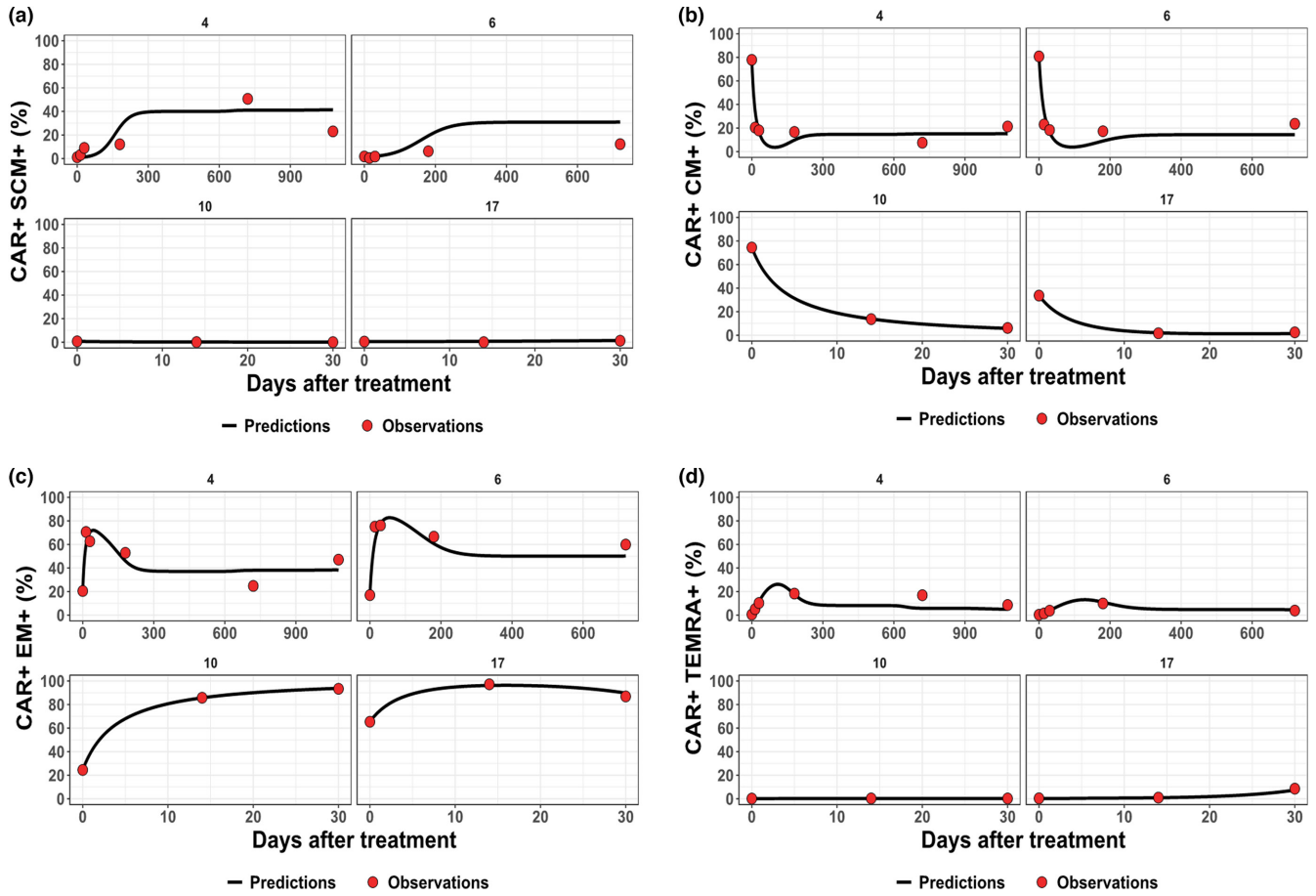

FIGURE 5 Simultaneous characterization of longitudinal changes in immunophenotypic composition post-infusion of CAT19 based anti-CD19 CAR T-cell therapy using a multiscale mechanistic CK-PD model. Observed (dots) and model fitted (lines) profiles for four patients (out of 14 pediatric ALL patients receiving CAR T-cell therapy), representing longitudinal changes in percentage of CAR+T_{SCM}+ (a), CAR+T_{CM}+ (b), CAR+T_{EM}+ (c) and CAR+T_{EFF}+ (d) populations in vivo. Patients 4 and 6 showed higher polyclonality and superior CAR T-cell persistence in comparison to patients 10 and 17, where persistence was limited. ALL, acute lymphocytic leukemia; CK, cellular kinetic; PD, pharmacodynamic; SCM, stem-cell memory; T_{CM}, T central memory cells; T_{EFF}, T effector cells; T_{EM}, T effector memory cells; T_{SCM}, stem cell memory cells.

T-cell products, either approved or under clinical development, which have evaluated a predefined ratio of CD4/CD8 subset.[14,30] These include infusion products with 1:1 ratio of CD4:CD8 subpopulations, such as Liso-cel (FDA approved) or Relmacel (National Medical Products Administration [Chinese drug agency] approved).[12,31] Therefore, toward development of mechanistic framework to describe CK of CAR T-cells, incorporating distinct behavior of these subsets become imperative.

Biasco et al. have recently demonstrated that the percentage of CAR+ T_{SCM} cells in the pre-infusion product and, polyclonality of CAR+T_{CM}+ and CAR+T_{EM}+ cells have critical contribution to the overall persistence of circulating CAR-T cells.[10] Similarly, Gattinoni et al. demonstrated that CAR+T_{SCM}+ immunophenotype is self-renewing and can generate T-memory and effector phenotypes to prolong tumor regressions.[32] Arcangeli et al. developed a protocol to expand and enrich CAR+T_{SCM}+ cells obtained from patients with B-cell acute ALL which demonstrated enhanced anticancer response in murine models.[15] The first-in-human trials of YTB323 (an investigational anti-CD19 CAR-T produced using T-Charge process with enriched CAR+T_{SCM}+ in the infusion product) showed similar expansion and clinical response at ~25-fold lower dose levels in comparison to clinically approved Tisagenlecleucel.[33] Similarly, P-MUC1C-ALLO1, a CAR T-cell product under clinical development against solid tumors, has enriched CAR+ T_{SCM+} cells in the infusion product.[34] Thus, mathematical models capturing these product characteristics are crucial for better understanding CK-PD relationship.

CAT19 CAR T-cells have ~40-fold faster K_{off} values than FMC63 based CAR T-cells enabling higher serial killing capacity, expansion (3–5 times increase in maximum plasma concentration and 0–28-day area under the concentration-time curve) and persistence.[20] Our in

vitro model estimated a 33-fold higher in vitro potency ($\mathbf{KC_{50}^{CAR-T}}$) for CAT19-based CAR T-cells compared to FMC63-based CAR T-cells, which is consistent with the hypothesized mechanism of action reported by Ghorashian et al.[20] Moreover, our in vivo model estimated superior expansion rate constant of CAR+CD8+ population of CAT-19-based CAR T-cell therapy compared to FMC63-based CAR T-cell therapy (5.3 $days^{-1}$ vs. 2.14 $days^{-1}$, respectively). When comparing the extent of persistence by quantitatively comparing "Rm" parameter estimate, our modeling analysis estimated superior persistence for CAT19 compared to FMC63 CAR-T cells (0.00003 day^{-1} vs. 0.000007 day^{-1}, respectively).

One of the further modifications within this mechanistic framework compared to prior published CK models for CAR T-cells has been to simultaneously characterize datasets from FCM and qPCR-based bioanalytical measurements. Each assay has its own pros and cons and can be used together to gain a holistic understanding of CAR T-cell CKs. Molecular assays like qPCR are often sensitive, reliable, and present less site-to-site variability. However, due to varying lymphocyte counts post-lymphodepletion chemotherapy, reportable units from PCR-based method generally overpredict CAR T-cell concentration in expansion and underpredict exposure during contraction. An FCM-based method could describe differential CKs of CAR T-cell subsets but is less sensitive and highly variable.[18,28] Further nuances between these two assays are described within the Appendix S1. The mass transfer within different compartments of our model(s) was concentration units (cells/μL) reportable from FCM bioanalytical readout. The FCM predictions were transformed to "copies/μg gDNA" units by using a linear relationship (Equation 1) integrating both CK readouts. Our linear model parameters (intercept and slope) estimated from CAT19-based CAR T-cell datasets were comparable to published relationships for tisagenlecleucel.[24] Of note, our results showed that this relationship adequately captured both CAR+CD3+ T-cells FCM and qPCR transgene copies/μg gDNA bioanalytical assays. Alternative methods could convert copies/μg gDNA to units of CAR+ cells/μL by quantitatively integrating information on white blood cells count, transduction efficiency, and mean vector copy number.[35] CK datasets derived from qPCR could be used to characterize the overall disposition of CAR T-cells, whereas CK datasets from FCM could be used to estimate parameters related to the differential disposition of CAR T-cell subsets and immunophenotypes thus providing holistic CAR T-cell exposure characterization.

While evaluating longitudinal changes in different immunophenotypic populations, it was observed that the T_{CM} transitions to T_{EM} and T_{EFF} during the CAR T-cell expansion stage. This observation was consistent across the patients (Figure 5) with "long term persistence" (ID4 and ID6) versus "short-term persistence" (ID10 and ID17). Therefore, a unified catenary model (described in step 3) was adopted from the work by Gattinoni et al.,[36] which could characterize one set of the differentiation rate constants to predict percentage changes in different immunophenotypes. In a low data environment with multiple readouts, our model provides adequate mechanistic interpretation of the observed dataset. The model incorporates polyclonality (i.e., increased clonal populations in cell product) as a categorical covariate influencing the differentiation rate constants for different immunophenotypes, demonstrating its role in long-term persistence. Polyclonality significantly reduced R_{m1}, R_{m2}, and R_{m3} by ~92%, 79%, and 81%, respectively, in CK datasets from responders and nonresponders, impacting persistence by enriching the circulating CAR+ T_{SCM+} population. However, the broader utility of this model is limited, until the model structure will be evaluated on a larger comprehensive dataset.

Although current modeling framework present significant improvements from previously published relationships, the analysis present several limitations. The cell killing potencies and binding interactions within the in vitro setting were assumed to be conserved in an in vivo scenario, which does not necessarily hold true. The digitized clinical CK-PD datasets lack patient-level covariate information, such as body weight, individual CD4/CD8 ratios, etc., which are imperative for adequate model building. Consequently, summary level information on body weight within a patient population, or average CD4:CD8 ratios were implemented. Often random variabilities (as described in the Method section) were implemented to account for (1) different disease indications, (2) varying summary statistics for FCM based readouts, (3) dealing with summary level patient−/product-characteristics, and (4) simultaneously integrating multiple bioanalytical measurements. Moreover, the final model (in step 3) was characterized on longitudinal changes of "percentage" of immunophenotypes and not absolute counts, which could affect parameter estimation. These limitations are more comprehensively discussed in the Appendix S1.

In conclusion, we have evolved our previously published multiscale mechanistic CK-PD model to successfully capture in vitro data (from CAT19 and FMC63-based CAR T-cells) and clinical CK datasets following administration of Liso-cel or CAT19-based CAR T-cells. The framework adequately described in vitro functionalities, incorporation of multiple bioanalytical techniques, CAR T-cell pre-infusion product-related attributes, such as CD4/CD8 subsets and immunophenotypes, along with their longitudinal changes post-infusion. Validation of this framework with additional clinical datasets will enable future optimization of product characteristics,

providing further mechanistic understanding of CK-PD relationships.

AUTHOR CONTRIBUTIONS

A.M.S. and A.P.S. wrote the manuscript. A.P.S. and G.M.M. designed the research. A.M.S. and A.P.S. performed the research. A.M.S. and A.P.S. analyzed the data.

ACKNOWLEDGMENTS

The authors would like to thank Dr. Christine Ward for critically reviewing this manuscript. The authors would also like to thank members within the Cell Therapy Clinical Pharmacology and modeling group, especially Thang Ho, Jia Li, Keyur Parmar, Angelia Wang, Erfan Maddah, and Iordanis Kesisoglou for continued discussion on the mathematical modeling aspects of cell therapies.

FUNDING INFORMATION

This work was funded by Takeda Development Center Americas, Inc.

CONFLICT OF INTEREST STATEMENT

A.P.S. and G.M.M. are employees and stockholders of Takeda Pharmaceuticals. A.M.S. was an employee of Takeda at the time of this work.

ORCID

Ahmed M. Salem https://orcid.org/0000-0002-2415-8801
Aman P. Singh https://orcid.org/0000-0002-1886-2624

REFERENCES

1. Approved Cellular and Gene Therapy Products. FDA 2021. https://www.fda.gov/vaccines-blood-biologics/cellular-gene-therapy-products/approved-cellular-and-gene-therapy-products. Accessed November 28, 2021
2. Beacon targeted therapies – make faster and better informed drug development decisions. https://beacon-intelligence.com/. Accessed May 7, 2022.
3. Albinger N, Hartmann J, Ullrich E. Current status and perspective of CAR-T and CAR-NK cell therapy trials in Germany. *Gene Ther*. 2021;28(9):513-527. doi:10.1038/s41434-021-00246-w
4. Liu C, Ayyar VS, Zheng X, et al. Model-based cellular kinetic analysis of chimeric antigen receptor-T cells in humans. *Clin Pharmacol Ther*. 2021;109(3):716-727. doi:10.1002/cpt.2040
5. Singh AP, Zheng X, Lin-Schmidt X, et al. Development of a quantitative relationship between CAR-affinity, antigen abundance, tumor cell depletion and CAR-T cell expansion using a multiscale systems PK-PD model. *mAbs*. 2020;12(1):1688616. doi:10.1080/19420862.2019.1688616
6. Rodriguez-Marquez P, Calleja-Cervantes ME, Serrano G, et al. CAR density influences antitumoral efficacy of BCMA CAR-T cells and correlates with clinical outcome. *Blood*. 2021;138(Suppl 1):735. doi:10.1182/blood-2021-148578
7. Hirayama AV, Gauthier J, Hay KA, et al. The response to lymphodepletion impacts PFS in patients with aggressive non-Hodgkin lymphoma treated with CD19 CAR T cells. *Blood*. 2019;133(17):1876-1887. doi:10.1182/blood-2018-11-887067
8. Finney OC, Brakke HM, Rawlings-Rhea S, et al. CD19 CAR T cell product and disease attributes predict leukemia remission durability. *J Clin Invest*. 2019;129(5):2123-2132. doi:10.1172/JCI125423
9. Turtle CJ, Hanafi LA, Berger C, et al. CD19 CAR-T cells of defined CD4+:CD8+ composition in adult B cell ALL patients. *J Clin Invest*. 2016;126(6):2123-2138. doi:10.1172/JCI85309
10. Biasco L, Izotova N, Rivat C, et al. Clonal expansion of T memory stem cells determines early anti-leukemic responses and long-term CAR T cell persistence in patients. *Nat Cancer*. 2021;2(6):629-642. doi:10.1038/s43018-021-00207-7
11. Mueller-Schoell A, Puebla-Osorio N, Michelet R, et al. Early survival prediction framework in CD19-specific CAR-T cell immunotherapy using a quantitative systems pharmacology model. *Cancer*. 2021;13(11):2782. doi:10.3390/cancers13112782
12. Research C for BE and. BREYANZI (lisocabtagene maraleucel). FDA 2021. https://www.fda.gov/vaccines-blood-biologics/cellular-gene-therapy-products/breyanzi-lisocabtagene-maraleucel. Accessed August 19, 2021.
13. Benmebarek MR, Karches CH, Cadilha BL, Lesch S, Endres S, Kobold S. Killing mechanisms of chimeric antigen receptor (CAR) T cells. *Int J Mol Sci*. 2019;20(6):E1283. doi:10.3390/ijms20061283
14. Cohen AD, Garfall AL, Stadtmauer EA, et al. B cell maturation antigen–specific CAR T cells are clinically active in multiple myeloma. *J Clin Invest*. 2019;129(6):2210-2221. doi:10.1172/JCI126397
15. Arcangeli S, Falcone L, Camisa B, et al. Next-generation manufacturing protocols enriching TSCM CAR T cells can overcome disease-specific T cell defects in cancer patients. *Front Immunol*. 2020;11:1217. doi:10.3389/fimmu.2020.01217
16. Chaudhury A, Zhu X, Chu L, et al. Chimeric antigen receptor T cell therapies: a review of cellular kinetic-pharmacodynamic modeling approaches. *J Clin Pharmacol*. 2020;60(S1):S147-S159. doi:10.1002/jcph.1691
17. Hardiansyah D, Ng CM. Quantitative systems pharmacology model of chimeric antigen receptor T-cell therapy. *Clin Transl Sci*. 2019;12(4):343-349. doi:10.1111/cts.12636
18. Stein AM, Grupp SA, Levine JE, et al. Tisagenlecleucel model-based cellular kinetic analysis of chimeric antigen receptor-T cells. *CPT Pharmacometrics Syst Pharmacol*. 2019;8(5):285-295. doi:10.1002/psp4.12388
19. Singh AP, Chen W, Zheng X, et al. Bench-to-bedside translation of chimeric antigen receptor (CAR) T cells using a multiscale systems pharmacokinetic-pharmacodynamic model: a case study with anti-BCMA CAR-T. *CPT Pharmacometrics Syst Pharmacol*. 2021;10(4):362-376. doi:10.1002/psp4.12598
20. Ghorashian S, Kramer AM, Onuoha S, et al. Enhanced CAR T cell expansion and prolonged persistence in pediatric patients with ALL treated with a low-affinity CD19 CAR. *Nat Med*. 2019;25(9):1408-1414. doi:10.1038/s41591-019-0549-5

21. Lugthart G, Albon SJ, Ricciardelli I, et al. Simultaneous generation of multivirus-specific and regulatory T cells for adoptive immunotherapy. *J Immunother*. 2012;35(1):42-53. doi:10.1097/CJI.0b013e31823569e2
22. Kaech SM, Wherry EJ, Ahmed R. Effector and memory T-cell differentiation: implications for vaccine development. *Nat Rev Immunol*. 2002;2(4):251-262. doi:10.1038/nri778
23. Westera L, Drylewicz J, den Braber I, et al. Closing the gap between T-cell life span estimates from stable isotope-labeling studies in mice and humans. *Blood*. 2013;122(13):2205-2212. doi:10.1182/blood-2013-03-488411
24. Research C for BE and. KYMRIAH (tisagenlecleucel). FDA 2021. https://www.fda.gov/vaccines-blood-biologics/cellular-gene-therapy-products/kymriah-tisagenlecleucel. Accessed August 23, 2021.
25. Abramson JS, Palomba ML, Gordon LI, et al. Lisocabtagene maraleucel for patients with relapsed or refractory large B-cell lymphomas (TRANSCEND NHL 001): a multicentre seamless design study. *Lancet*. 2020;396(10254):839-852. doi:10.1016/S0140-6736(20)31366-0
26. Beal SL. Ways to fit a PK model with some data below the quantification limit. *J Pharmacokinet Pharmacodyn*. 2001;28(5):481-504. doi:10.1023/A:1012299115260
27. Marofi F, Motavalli R, Safonov VA, et al. CAR T cells in solid tumors: challenges and opportunities. *Stem Cell Res Ther*. 2021;12(1):81. doi:10.1186/s13287-020-02128-1
28. Mueller KT, Maude SL, Porter DL, et al. Cellular kinetics of CTL019 in relapsed/refractory B-cell acute lymphoblastic leukemia and chronic lymphocytic leukemia. *Blood*. 2017;130(21):2317-2325. doi:10.1182/blood-2017-06-786129
29. Macallan DC, Asquith B, Irvine AJ, et al. Measurement and modeling of human T cell kinetics. *Eur J Immunol*. 2003;33(8):2316-2326. doi:10.1002/eji.200323763
30. Abramson JS, Gordon LI, Palomba ML, et al. Updated safety and long term clinical outcomes in TRANSCEND NHL 001, pivotal trial of lisocabtagene maraleucel (JCAR017) in R/R aggressive NHL. *JCO*. 2018;36(15_suppl):7505. doi:10.1200/JCO.2018.36.15_suppl.7505
31. Ying Z, Yang H, Guo Y, et al. Relmacabtagene autoleucel (relma-cel) CD19 CAR-T therapy for adults with heavily pretreated relapsed/refractory large B-cell lymphoma in China. *Cancer Med*. 2021;10(3):999-1011. doi:10.1002/cam4.3686
32. Gattinoni L, Speiser DE, Lichterfeld M, Bonini C. T memory stem cells in health and disease. *Nat Med*. 2017;23(1):18-27. doi:10.1038/nm.4241
33. Flinn IW, Jaeger U, Shah NN, et al. A first-in-human study of YTB323, a novel, autologous CD19-directed CAR-T cell therapy manufactured using the novel T-charge TM platform, for the treatment of patients (Pts) with relapsed/refractory (r/r) diffuse large B-cell lymphoma (DLBCL). *Blood*. 2021;138(Suppl 1):740. doi:10.1182/blood-2021-146268
34. Kozlowska A, Zhang Y, Fritz J, et al. 120 P-MUC1C-ALLO1: an allogeneic car-t for multiple solid tumor indications. *J Immunother Cancer*. 2020;8(Suppl 3):A73. doi:10.1136/jitc-2020-SITC2020.0120
35. Chaudhury A, Stein A, Grupp S, et al. Abstract 509: Conversion of cellular kinetic data for chimeric antigen receptor T-cell therapy (CAR-T) into interpretable units. *Cancer Res*. 2021;81(13 Supplement):509. doi:10.1158/1538-7445.AM2021-509
36. Gattinoni L, Lugli E, Ji Y, et al. A human memory T cell subset with stem cell-like properties. *Nat Med*. 2011;17(10):1290-1297. doi:10.1038/nm.2446
37. German Collection of Microorganisms and Cell Cultures GmbH: Details. https://www.dsmz.de/collection/catalogue/details/culture/ACC-140. Accessed August 22, 2021
38. Friedman KM, Garrett TE, Evans JW, et al. Effective targeting of multiple B-cell maturation antigen-expressing hematological malignances by anti-B-cell maturation antigen chimeric antigen receptor T cells. *Hum Gene Ther*. 2018;29(5):585-601. doi:10.1089/hum.2018.001
39. Cabezudo E, Carrara P, Morilla R, Matutes E. Quantitative analysis of CD79b, CD5 and CD19 in mature B-cell lymphoproliferative disorders. *Haematologica*. 1999;84(5):413-418.
40. Nombela-Arrieta C, Manz MG. Quantification and three-dimensional microanatomical organization of the bone marrow. *Blood Adv*. 2017;1(6):407-416. doi:10.1182/bloodadvances.2016003194
41. Horna P, Nowakowski G, Endell J, Boxhammer R. Comparative assessment of surface CD19 and CD20 expression on B-cell lymphomas from clinical biopsies: implications for targeted therapies. *Blood*. 2019;134(Suppl 1):5345. doi:10.1182/blood-2019-129600
42. Roesch K, Hasenclever D, Scholz M. Modelling lymphoma therapy and outcome. *Bull Math Biol*. 2014;76(2):401-430. doi:10.1007/s11538-013-9925-3
43. Skipper HE, Perry S. Kinetics of normal and leukemic leukocyte populations and relevance to chemotherapy. *Cancer Res*. 1970;30(6):1883-1897.
44. Savvopoulos S, Misener R, Panoskaltsis N, Pistikopoulos EN, Mantalaris A. A personalized framework for dynamic modeling of disease trajectories in chronic lymphocytic leukemia. *IEEE Trans Biomed Eng*. 2016;63(11):2396-2404. doi:10.1109/TBME.2016.2533658
45. Amin HM, Yang Y, Shen Y, et al. Having a higher blast percentage in circulation than bone marrow: clinical implications in myelodysplastic syndrome and acute lymphoid and myeloid leukemias. *Leukemia*. 2005;19(9):1567-1572. doi:10.1038/sj.leu.2403876
46. Ogasawara K, Dodds M, Mack T, Lymp J, Dell'Aringa J, Smith J. Population cellular kinetics of lisocabtagene maraleucel, an autologous CD19-directed chimeric antigen receptor T-cell product, in patients with relapsed/refractory large B-cell lymphoma. *Clin Pharmacokinet*. 2021;60(12):1621-1633. doi:10.1007/s40262-021-01039-5
47. Yamamura R, Yamane T, Hino M, et al. Possible automatic cell classification of bone marrow aspirate using the CELL-DYN 4000 automatic blood cell analyzer. *J Clin Lab Anal*. 2002;16(2):86-90. doi:10.1002/jcla.10025
48. Zhu M, Kratzer A, Johnson J, et al. Blinatumomab pharmacodynamics and exposure-response relationships in relapsed/refractory acute lymphoblastic leukemia. *J Clin Pharmacol*. 2018;58(2):168-179. doi:10.1002/jcph.1006
49. Hirt A, Schmid AM, Ammann RA, Leibundgut K. In pediatric lymphoblastic leukemia of B-cell origin, a small population of primitive blast cells is noncycling, suggesting them to be leukemia stem cell candidates. *Pediatr Res*. 2011;69(3):194-199. doi:10.1203/PDR.0b013e3182092716
50. Dai Q, Zhang G, Yang H, et al. Clinical features and outcome of pediatric acute lymphoblastic leukemia with low

peripheral blood blast cell count at diagnosis. *Medicine (Baltimore)*. 2021;100(4):e24518. doi:10.1097/MD.0000000000024518

SUPPORTING INFORMATION

Additional supporting information can be found online in the Supporting Information section at the end of this article.

How to cite this article: Salem AM, Mugundu GM, Singh AP. Development of a multiscale mechanistic modeling framework integrating differential cellular kinetics of CAR T-cell subsets and immunophenotypes in cancer patients. *CPT Pharmacometrics Syst Pharmacol*. 2023;12:1285-1304. doi:10.1002/psp4.13009